nature genetics

Signaling from maize organ primordia via FASCIATED EAR3 regulates stem cell proliferation and yield traits

Byoung Il Je[1], Jeremy Gruel[2,8], Young Koung Lee[1,8], Peter Bommert[1], Edgar Demesa Arevalo[1], Andrea L Eveland[1,7], Qingyu Wu[1], Alexander Goldshmidt[1], Robert Meeley[3], Madelaine Bartlett[4], Mai Komatsu[5], Hajime Sakai[5], Henrik Jönsson[2,6] & David Jackson[1]

Shoot apical meristems are stem cell niches that balance proliferation with the incorporation of daughter cells into organ primordia. This balance is maintained by CLAVATA–WUSCHEL feedback signaling between the stem cells at the tip of the meristem and the underlying organizing center. Signals that provide feedback from organ primordia to control the stem cell niche in plants have also been hypothesized, but their identities are unknown. Here we report FASCIATED EAR3 (FEA3), a leucine-rich-repeat receptor that functions in stem cell control and responds to a CLAVATA3/ESR-related (CLE) peptide expressed in organ primordia. We modeled our results to propose a regulatory system that transmits signals from differentiating cells in organ primordia back to the stem cell niche and that appears to function broadly in the plant kingdom. Furthermore, we demonstrate an application of this new signaling feedback, by showing that weak alleles of *fea3* enhance hybrid maize yield traits.

Stem cells occur in niches, specialized microdomains where proliferation of pluripotent cells is controlled by signals from neighboring cells[1,2]. In plants, for example, the WUSCHEL (WUS) transcription factor promotes stem cell fate and is expressed in organizing center cells below stem cells. WUS activates *CLAVATA* (*CLV*) gene expression and the CLV signaling pathway[3–5]. As a result, the CLV3 peptide ligand is secreted from stem cells at the tip of the shoot apical meristem (SAM), is perceived by leucine-rich-repeat (LRR) receptors, such as CLV1, which is expressed in and above the *WUS* organizing center cell domain, and signals in a feedback loop to repress *WUS* expression[3–5].

Although such feedback systems are well described in animals and plants, it is not known whether or how signals expressed in differentiating progeny cells also provide feedback to control the stem cell niche. In plants, such signals have been hypothesized[6–8], and, consistent with this idea, the inhibition of primordium growth leads to SAM enlargement[9]. However, the underlying molecular mechanism(s) are unknown. To search for factors controlling stem cell proliferation, we focused on maize *fasciated ear* (*fea*) mutants, some of which correspond to CLV receptors already described in eudicots[10–13]. Here we provide evidence to support a new receptor–ligand signaling pathway that acts to restrict stem cell proliferation using a signal expressed in differentiating cells in organ primordia.

RESULTS

fea3 mutants have enlarged and fasciated meristems

The *fea3* mutant allele arose in an irradiation mutagenesis screen and was introgressed into the B73 background. *fea3* vegetative SAMs were wider (mean diameter of 150 ± 4.5 µm) than the SAMs of their wild-type siblings (128 ± 5.8 µm; *P* value < 0.001, two-tailed *t* test) (**Fig. 1a**,**b**). Despite the larger size of the *fea3* SAM, its identity and organization were not adversely affected, as shown by *KNOTTED1* expression (**Supplementary Fig. 1a**)[14]. *fea3* mutants had prominent inflorescence defects, including thick tassels and strongly fasciated ears with increased seed row number, resembling maize *clv* mutants (**Fig. 1c–j**)[10,13], although overall plant stature was normal (**Supplementary Fig. 1b**). In contrast to maize *clv* receptor mutants, however, spikelet and flower development were normal in *fea3* mutants (**Supplementary Fig. 1c**,**d**)[10,13]. Fasciated ears and thick tassels result from increased stem cell proliferation in inflorescence meristems. We found that *fea3* tassel inflorescence meristems were larger than wild-type ones (**Fig. 1c**,**d**). *fea3* ear inflorescence meristems were also enlarged and became more severely affected during development (**Fig. 1f–i**).

FEA3, a transmembrane receptor, is expressed in the SAM

We mapped *fea3* to a region containing ~20 genes (**Fig. 1k**), including one that encoded an LRR-receptor-like protein. On the basis of similar phenotypes for related genes[10,13], we sequenced this locus from *fea3-0* and found a retrotransposon fragment inserted in the second exon, introducing a premature stop codon (**Supplementary Fig. 2a**). Three additional *fea3* alleles from a targeted ethylmethane sulfonate (EMS) screen encoded amino acid substitutions relative to the progenitor (**Fig. 1l** and **Supplementary Fig. 2b**). Therefore, *FEA3* encodes an LRR-receptor-like protein, with a predicted signal peptide followed by 12 LRRs, a transmembrane domain, and a short cytoplasmic tail,

[1]Cold Spring Harbor Laboratory, Cold Spring Harbor, New York, New York, USA. [2]Sainsbury Laboratory, University of Cambridge, Cambridge, UK. [3]Agricultural Biotechnology, DuPont Pioneer, Johnston, Iowa, USA. [4]Department of Biology, University of Massachusetts, Amherst, Massachusetts, USA. [5]Agricultural Biotechnology, DuPont Pioneer, Wilmington, Delaware, USA. [6]Computational Biology and Biological Physics Group, Lund University, Lund, Sweden. [7]Present address: Donald Danforth Plant Science Center, St. Louis, Missouri, USA. [8]These authors contributed equally to this work. Correspondence should be addressed to D.J. (jacksond@cshl.edu).

Received 1 December 2015; accepted 13 April 2016; published online 16 May 2016; doi:10.1038/ng.3567

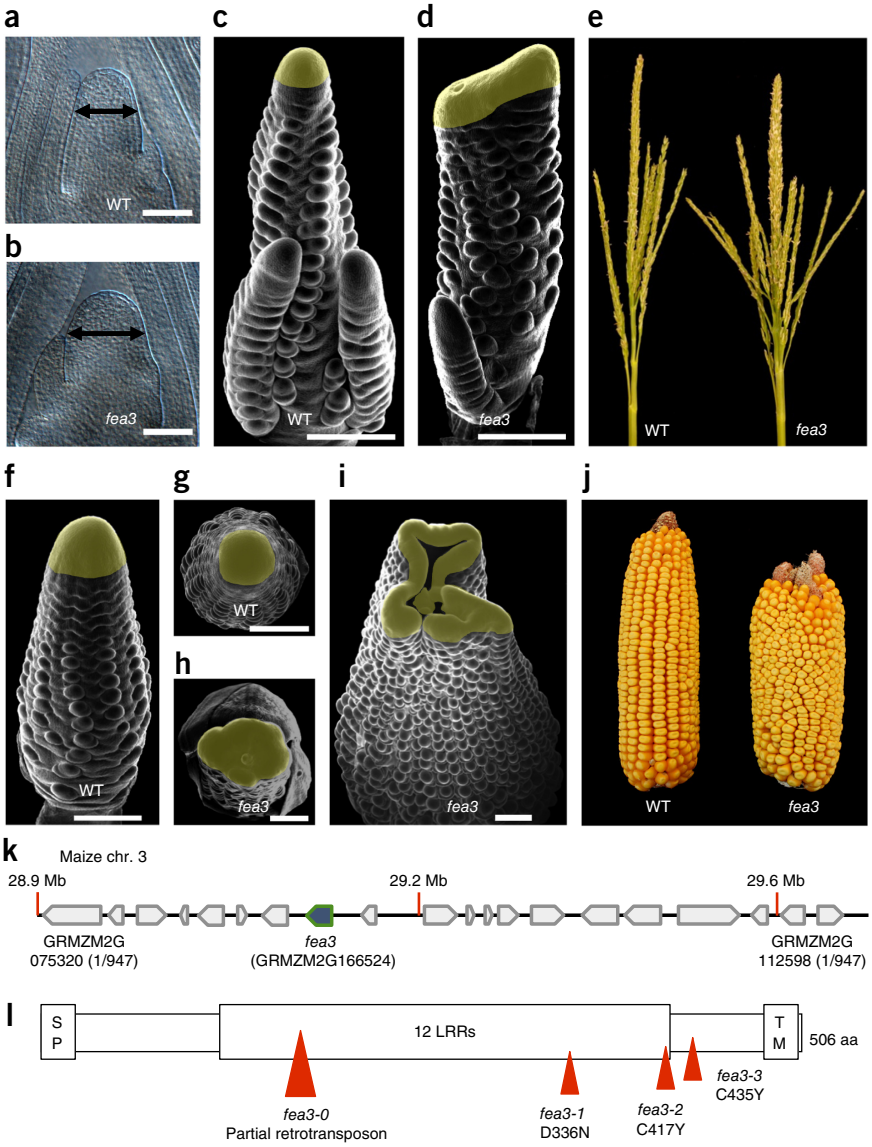

Figure 1 *fea3* mutant phenotypes and gene identification. (**a**,**b**) Cleared SAMs from wild-type (WT) (**a**) and *fea3* (**b**) plants. The *fea3* SAM has a larger diameter (double-headed arrows). (**c**,**d**) Scanning electron microscopy images of wild-type (**c**) and *fea3* (**d**) tassel primordia (inflorescence meristems in yellow). The *fea3* tassel shows an enlarged inflorescence meristem. (**e**) Wild-type (left) and *fea3* (right) tassels. The *fea3* tassel has a thicker appearance. (**f**,**g**) Side (**f**) and top–down (**g**) scanning electron microscopy views of wild-type ear primordia. (**h**,**i**) Top–down views of early-stage (**h**) and late-stage (**i**) *fea3* ear primordia, showing enlargement and fasciation of inflorescence meristems. (**j**) Wild-type ear (left) shows regular kernel rows; *fea3* ear (right) shows fasciation and irregular rows. (**k**) Map-based cloning of *fea3*. The number of recombinants among F_2 individuals is indicated. (**l**) FEA3 is a predicted receptor-like protein with a signal peptide (SP) followed by 12 LRRs and a transmembrane (TM) domain. The positions of the *fea3-0* insertion and the EMS alleles are shown. Scale bars: 100 µm in **a** and **b**, 500 µm in **c**, **d**, and **f**–**i**.

lacking any kinase or other predicted signaling domain (**Fig. 1l**).

FEA3 expression was enriched in meristems (**Supplementary Fig. 2c**), and *in situ* hybridization detected expression in the inner cells of the vegetative SAM central zone and in cells below the central zone, as well as in leaf primordia (**Fig. 2a** and **Supplementary Fig. 2d**–**f**). *FEA3* was also expressed in the central region of ear spikelet meristems (**Supplementary Fig. 2f**). We next expressed FEA3-RFP fusions, with expression driven by the endogenous *FEA3* promoter (p*FEA3*::*FEA3-RFP*). RFP was fused after the signal peptide in one construct and at the C terminus of FEA3 in another (**Supplementary Fig. 3a**). The expression of both transgene constructs rescued *fea3* phenotypes (**Supplementary Fig. 3b**). FEA3-RFP accumulated in the central region of the SAM (**Supplementary Fig. 3c**), consistent with the *in situ* hybridization data, but was not enriched in the plasma membrane, which might reflect endocytic trafficking, as reported for CLV1 (ref. 15). We therefore treated with D15 peptide, an inhibitor of endocytosis[16]. With this treatment, FEA3-RFP became enriched at the cell periphery after 2 h (**Fig. 2b** and **Supplementary Fig. 3d**), and we confirmed its plasma membrane localization biochemically (**Supplementary Fig. 3e**). FEA3-RFP was detected in the inner layers of the inflorescence SAM (**Fig. 2b**) in a pattern similar to that observed for *FEA3* mRNA in the vegetative SAM (**Fig. 2a**), with expression ranging from the fifth to sixth layer of cells below the first layer (L1) to the twelfth to thirteenth layer. Expression was also found in tassel and ear inflorescence meristems, in spikelet meristems (**Supplementary Fig. 3f**–**h**), in cells above the quiescent center of the root (**Supplementary Fig. 3i**), and in leaf primordia (**Fig. 2b** (inset) and **Supplementary Fig. 3j**).

Because FEA3 was expressed lower down in the SAM than known *Arabidopsis thaliana* CLV signaling components[12,17], we investigated its effect on *WUS* expression. CLV3 and CLV1 are expressed above and overlapping with the *WUS* domain, and WUS expression expands upward in *clv* mutants[3,4]. We generated a maize *WUS* reporter using the *ZmWUS1* promoter and 3′ region[18] to drive expression of nuclear RFP (p*ZmWUS1*::*NLS.RFP*). In wild-type plants, the reporter construct was expressed in the predicted organizing center, as expected, with expression starting 4–5 cell layers below layer L1 and extending down ~5 cell layers (**Fig. 2c**), in a domain that largely overlapped with that of FEA3-RFP, although FEA3-RFP expression also extended lower, below the organizing center. Strikingly, nuclear RFP expression expanded downward in *fea3* plants, below the presumptive organizing center (**Fig. 2d**). Interestingly, despite this obvious downward spread of reporter expression from the *ZmWUS1* promoter, there was no expansion into the upper layers of the SAM (**Fig. 2d**), suggesting that FEA3 functions to suppress *ZmWUS1* expression specifically in the region below the organizing center.

fea3 is resistant to a new CLE peptide, ZmFCP1

As FEA3 encodes an LRR-receptor-like protein, we reasoned that it might perceive CLV3 or a related CLV3/EMBRYO-SURROUNDING REGION (CLE) peptide. We therefore treated seedlings with peptides and measured inhibition of root growth[19,20]. Maize roots treated with a control, scrambled CLV3 peptide (sCLV3) grew normally

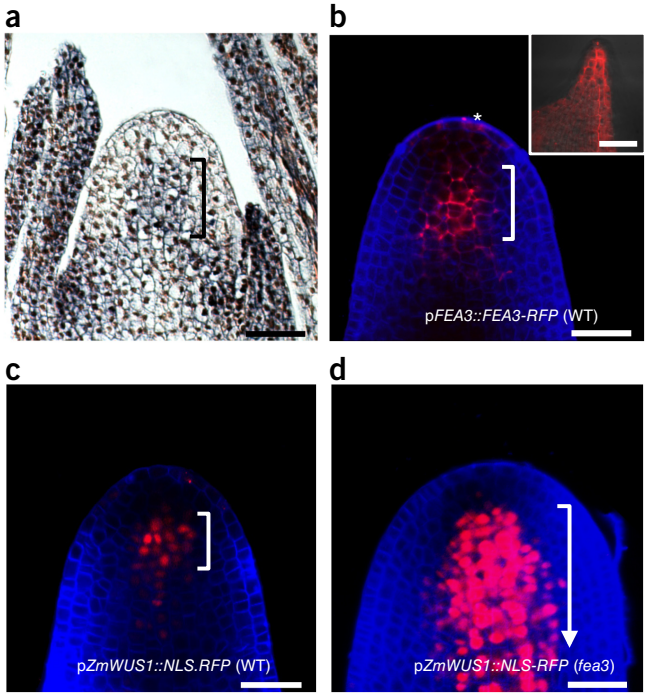

Figure 2 Expression of *FEA3* and *ZmWUS1*. (**a**) *In situ* hybridization for *FEA3* shows expression in lower layers of the vegetative SAM corresponding to the predicted organizing center (bracket) and below. (**b**) In the inflorescence apex, FEA3-RFP (red) is similarly expressed. Note that the diffuse and speckled red signal in the L1 SAM layer (asterisk) is background autofluorescence. FEA3-RFP is also expressed in leaf primordia (inset). (**c**) An inflorescence transition stage SAM shows nuclear RFP expression from the *ZmWUS1* promoter (red) in the presumptive organizing center in a wild-type plant. (**d**) Nuclear RFP expression from the *ZmWUS1* promoter expands downward in a *fea3* mutant plant. Tissues in **b**–**d** were counterstained (blue) with the calcofluor white cell wall marker (confocal microscopy). Scale bars, 50 μm.

but were inhibited in the presence of CLV3 (ref. 21). However, *fea2* (maize *clv2*) mutant roots showed resistance to CLV3 peptide, suggesting that FEA2 functions in CLV3 perception. *fea3* mutants, however, did not show resistance to CLV3 (**Supplementary Fig. 4**), suggesting that FEA3 might perceive a different ligand. We constructed a phylogeny of maize CLE peptides[22] (**Supplementary Fig. 5**) and found that ZmCLE7, ZmCLE14, and rice FLORAL ORGAN NUMBER 2 (FON2)[23] were the most closely related to CLV3. In a sister clade, we identified a gene orthologous to rice *FON2-LIKE CLE PROTEIN 1* (*FCP1*)[24], which we named *ZmFCP1*. Rice *fcp1* misexpression lines have meristem size phenotypes, but genetic evidence suggests that the rice *CLV1* ortholog does not encode the FCP1 receptor[24]. The predicted peptides encoded by these genes and additional related peptides were tested, and each of them inhibited wild-type root growth, similar to CLV3. Interestingly, *fea3* roots showed resistance only to ZmFCP1 peptide (**Supplementary Fig. 6**). We next asked whether FEA3 showed similar specificity for ZmFCP1 peptide in the shoot, by measuring the effect of ZmFCP1 peptide on SAM size in cultured embryos[21]. Wild-type embryos grew normally in the presence of the sCLV3 peptide control but showed a significant decrease ($P < 0.001$) in SAM size in the presence of ZmFCP1 or related peptides, such as ZmCLE7 or ZmCLE14, whereas *fea3* embryos again showed resistance only to ZmFCP1 (**Fig. 3a**,**b**). These findings suggest that FEA3 functions as a receptor in perception

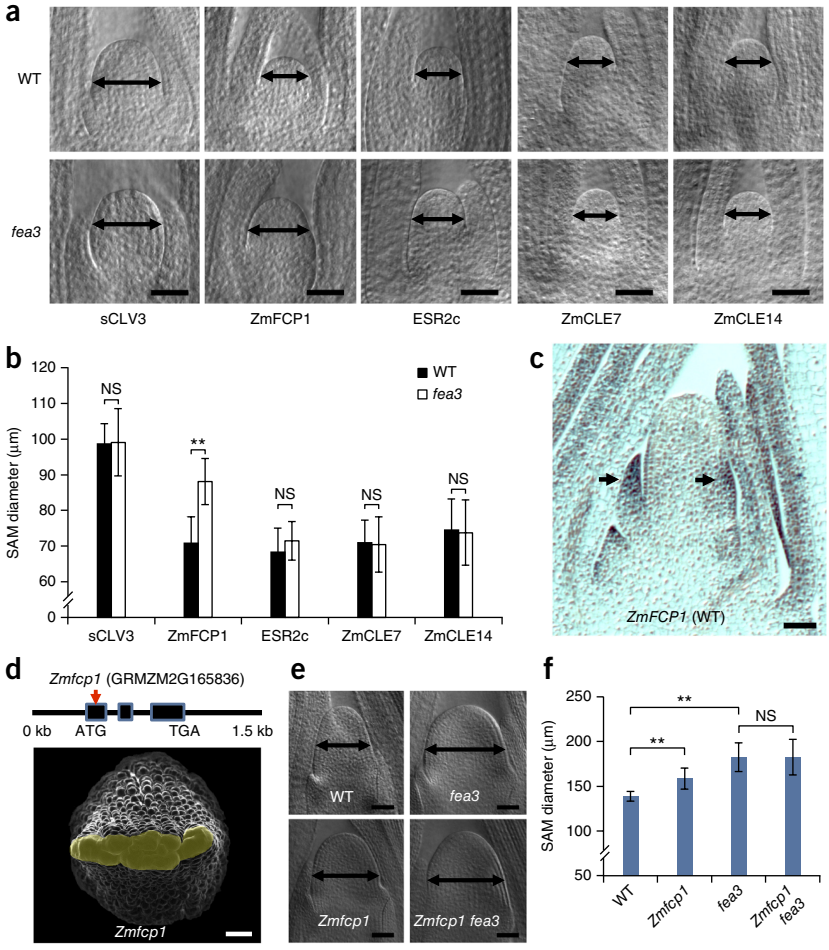

Figure 3 Interactions between FEA3 and its putative ligand, ZmFCP1. (**a**,**b**) Wild-type and *fea3* embryos were cultured with control, scrambled peptide (sCLV3) or with ZmFCP1, ESR2c, ZmCLE7, or ZmCLE14. Wild-type SAM growth (double-headed arrows) was strongly inhibited by all peptides except sCLV3, and *fea3* growth was insensitive only to ZmFCP1 (**a**); SAM diameter was quantified (**b**). (**c**) *In situ* hybridization for *ZmFCP1* in a wild-type SAM. Expression was specific to primordia (arrows). (**d**) Top, schematic of the *Zmfcp1* mutant allele. The red arrow indicates the position of the *Mutator* transposon insertion downstream of the ATG codon in the first exon. Bottom, *Zmfcp1* mutants have a fasciated ear phenotype, as seen in the top–down scanning electron microscopy view. (**e**,**f**) Cleared SAMs from wild-type, *fea3*, *Zmfcp1*, and double-mutant plants. SAMs from *fea3* and *Zmfcp1* plants were significantly wider than in wild type (double-headed arrows), but SAM size was not significantly different in the double mutant relative to the *fea3* mutant (**e**); SAM diameter was quantified (**f**). Scale bars: 500 μm in **d**, 50 μm in **a**, **c**, and **e**. $n = 20$ for each genotype in **b** and **f**. Data in **b** and **f** are shown as means ± s.d.: $^{**}P < 0.001$, two-tailed, two-sample *t* test; NS, not significant.

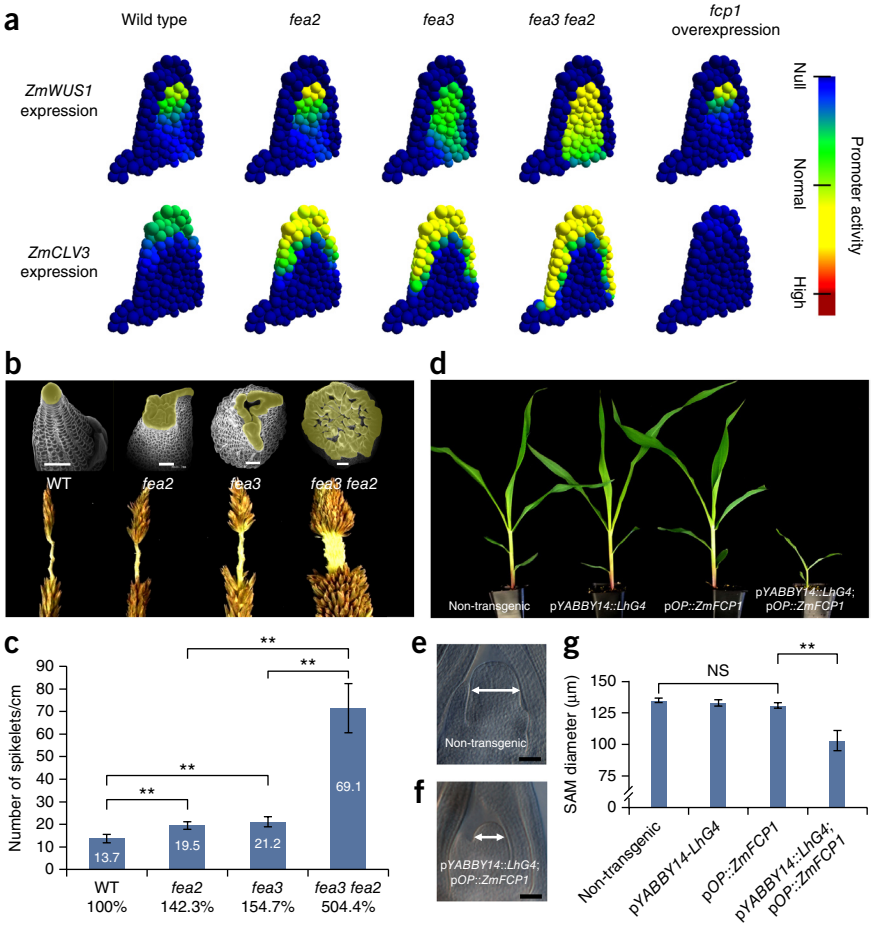

Figure 4 Computational model and tests of FEA3 function. (**a**) A computational model predicting the effect of genetic perturbations on hypothetical *ZmWUS1* and *ZmCLV3* expression domains and feedback upregulation of *ZmCLV3*. (**b**–**g**) We tested the model predictions by characterizing *fea3 fea2* double mutants (**b**,**c**) and examining the effect of *ZmFCP1* overexpression from organ primordia (**d**–**g**). (**b**,**c**) The *fea2* and *fea3* alleles act synergistically in double mutants with respect to ear meristems (top; scanning electron microscopy images) and tassels (bottom) (**b**); tassel spikelet density was quantified (**c**). (**d**–**g**) Transactivated overexpression of *ZmFCP1* in primordia (**d**) led to a severe reduction in SAM size (**f**), as compared to non-transgenic (**e**); SAM diameter was quantified (**g**). Scale bars: 500 µm in **b**, 50 µm in **e** and **f**. $n = 20$ (**c**) and 15 (**g**) plants for each genotype. Data in **c** and **g** are shown as means ± s.d.: $^{**}P < 0.001$, two-tailed, two-sample *t* test; NS, not significant.

of the ZmFCP1 peptide. In contrast, *fea2* mutants showed resistance to a broader class of peptides, including CLV3, ZmFCP1, and ESR2c, consistent with findings for *clv2* in *Arabidopsis* (**Supplementary Fig. 6b**).

In *Arabidopsis*, *CLV3* is expressed in stem cells at the tip of the SAM, and it is believed that CLV3 peptide moves down toward the organizing center to restrict WUS expression[3–5], although the peptide itself has never been localized *in vivo*. In contrast to *CLV3*, we found that *ZmFCP1* was not expressed in the SAM but was expressed in leaf primordia and in cells flanking the SAM that are destined to be incorporated into primordia (**Fig. 3c**; for comparison of *FEA3* and *ZmFCP1* expression, see **Supplementary Fig. 7a**,**b**). We next obtained a line with a *Mutator* insertion[25] in the first exon of *ZmFCP1*, and homozygous mutants had a fasciated ear phenotype (**Fig. 3d**). *Zmfcp1* vegetative SAMs were also wider than normal (mean diameter of 167 ± 10.4 µm, as compared to 142 ± 7.5 µm for wild-type siblings; *P* value < 0.001). *fea3* was epistatic to *Zmfcp1*, as double mutants had the same SAM size as *fea3* single mutants (**Fig. 3e**,**f**).

In summary, our data support the idea that *ZmFCP1* controls SAM size in the same pathway as *FEA3*. We propose a model in which

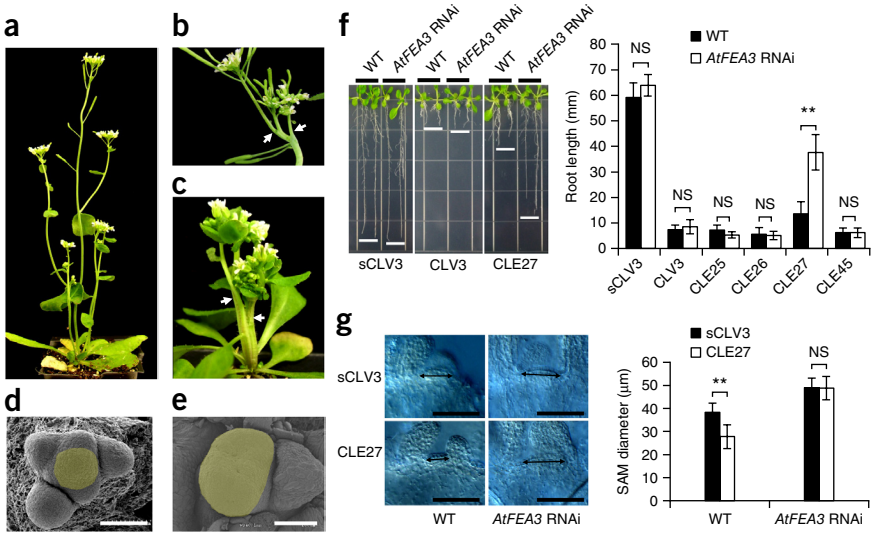

Figure 5 *Arabidopsis FEA3* RNAi mutants are fasciated. (**a**,**d**) Wild-type line Landsberg erecta (Ler). Photograph of a wild-type plant (**a**) and a scanning electron microscopy image of a wild-type SAM (yellow) (**d**). (**b**,**c**,**e**) *AtFEA3* RNAi transgenic plants. *AtFEA3* RNAi plants are fasciated, with split inflorescence stems (arrows) (**b**,**c**), and the scanning electron microscopy image shows that the SAM is enlarged in these plants (**e**). (**f**) In wild-type plants, root growth was strongly inhibited by CLE peptides but not by sCLV3 control peptide. In contrast, the *AtFEA3* RNAi lines showed resistance to CLE27. Root tips are marked by white bars (left); root growth was quantified (right). The experiment was performed for $n = 20$ plants per genotype and treatment condition. (**g**) Wild-type SAM growth was significantly inhibited by treatment with CLE27 peptide, but *AtFEA3* RNAi plants were resistant to CLE27 (left images show cleared SAMs; SAM diameter was quantified, right). The experiment was performed for $n = 19$ plants per genotype and treatment condition. Scale bars: 50 µm in **d** and **g**, 200 µm in **e**. In the graphs in **f** and **g**, data are shown as means ± s.d.: $^{**}P < 0.001$, two-tailed, two-sample *t* test; NS, not significant.

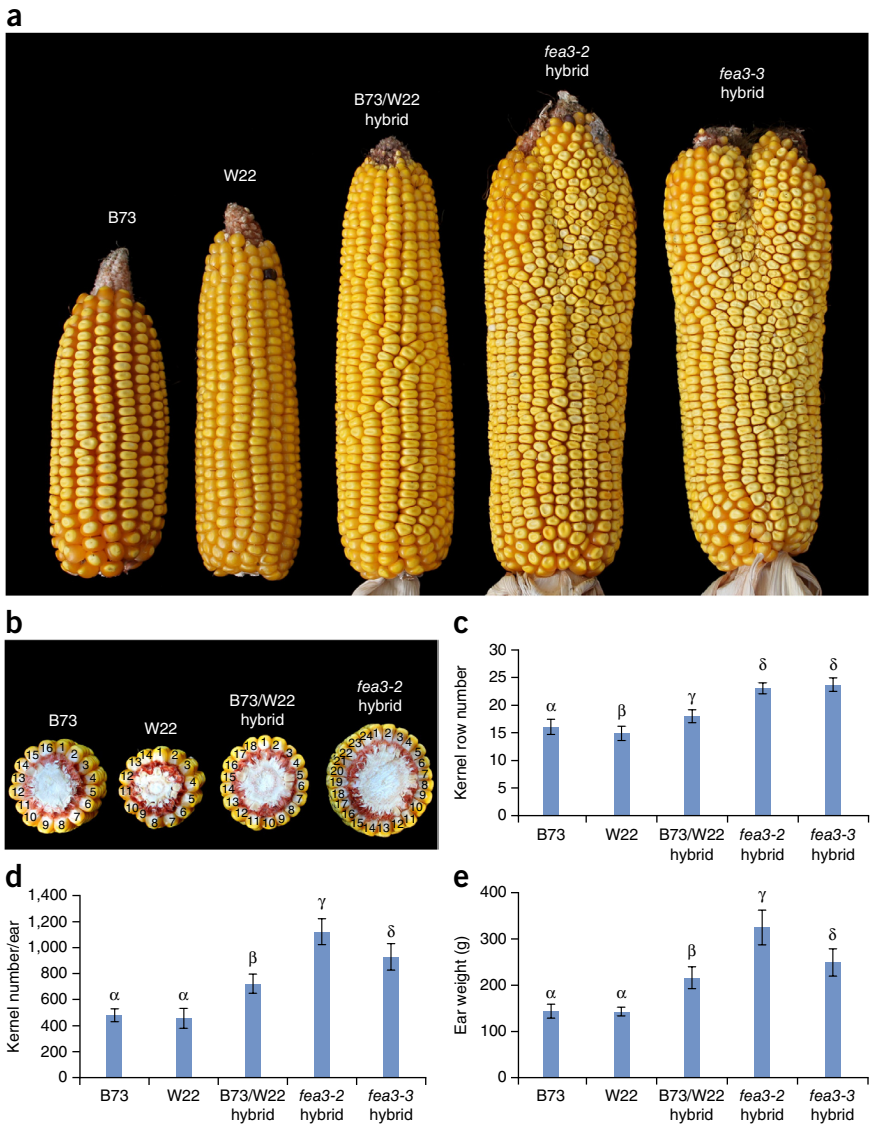

Figure 6 Yield traits for weak *fea3* alleles. (**a**–**c**) Photographs of the ears from inbred or hybrid *fea3* heterozygous (B73/W22) or homozygous plants are shown (**a**), with kernel rows numbered (**b**) and quantified (**c**). Hybrids with weak *fea3* alleles had longer and wider ears than normal hybrids and had increased kernel row numbers. (**d**,**e**) Kernel number per ear (**d**) and ear weight (**e**) were also significantly higher in *fea3-2* and *fea3-3* hybrids as compared to normal hybrids. $n = 20$ plants per genotype; the first ear of each plant was analyzed. Data are shown as means ± s.d. Greek letters indicate significant differences; bars with the same letter are not significantly different.

ZmFCP1 peptide is produced from differentiating primordium cells and suppresses WUS expression and stem cell proliferation via the FEA3 receptor in the SAM. This model is supported by FEA3 and ZmFCP1 expression patterns and by our observation of downward spread of WUS in *fea3* mutant meristems.

Computational modeling of *FEA3–ZmFCP1* interactions

To understand the spatial patterning resulting from this new CLE peptide–receptor signaling, we integrated the *FEA3–ZmFCP1* regulation of *ZmWUS1* with the canonical *CLV3–WUS* feedback loop, recently modeled in *Arabidopsis*[26–28] (Online Methods and **Supplementary Figs. 7–12**). We assumed that certain functions and expression domains, such as for the cytokinin pathway genes or *WUS* and its activation of stem cells, are conserved in maize, although some of these have not yet been demonstrated. On a three-dimensional geometry representing the maize SAM and two primordia (**Supplementary Figs. 7–12**), the model reproduced the wild-type expression domain of *ZmWUS1* and generated a stem cell domain expressing a hypothetical *ZmCLV3* ortholog in the central zone (**Fig. 4a**). The model predicts that alteration in the FEA3 receptor, which responds to a CLE signal from the leaf primordia, leads to downward spread of *ZmWUS1* expression and that this change in expression would lead to an expansion of the stem cell population and upregulation of *CLV3* expression, which has previously been correlated with fasciation[3,29]. We tested this model in three ways. First, we measured expression of *ZmCLE7*, a maize ortholog of *CLV3* (**Supplementary Fig. 5**), and found an increase in expression in the meristem tips of *fea3* mutants (**Supplementary Fig. 13**), consistent with our predictions. Next, we characterized *fea3 fea2* double mutants and found that the phenotypes of the double mutants were highly synergistic (P value < 0.001) with respect to ear inflorescence meristem size and tassel spikelet density, a proxy for tassel inflorescence meristem size[21] (**Fig. 4b**,**c**). This result suggests that *FEA3* and *FEA2* act in different pathways that may converge on the same downstream target, consistent with our model (**Fig. 4a**). As a third test of the model, we overexpressed *ZmFCP1* in organ primordia using a two-component driver system[30]. We used a p*YABBY14*::*LhG4* line to drive primordium-specific expression in a p*Op*::*ZmFCP1* responder line. Driver specificity was confirmed by detection of nuclear RFP expression from p*Op*::*NLS.RFP* only in primordia (**Supplementary Fig. 14a**,**b**), and we measured SAM size in segregating families. Plants carrying either the driver or responder component alone had normal SAM size, but plants carrying both constructs showed strong inhibition of SAM growth (**Fig. 4d–g**); *ZmFCP1* overexpression was confirmed by qRT–PCR (**Supplementary Fig. 14c**). These tests of the model support the idea that ZmFCP1 signaling from differentiating primordia is sufficient to suppress stem cell proliferation, consistent with the reduced *WUS* expression domain in the *fcp1* overexpression model (**Fig. 4a**).

Arabidopsis FEA3 ortholog mutants are also fasciated

To ask whether *FEA3* is specific to maize, we characterized its three potential orthologs, *At1g68780*, *At1g13230*, and *At3g25670*, in *Arabidopsis* (**Supplementary Fig. 5**). Predicted null transgenic DNA (T-DNA) mutants of the first two orthologs showed no obvious aberrant phenotype, even when combined in a double mutant. We therefore generated artificial microRNA (miRNA) (**Supplementary Fig. 15a**,**b**) or RNA interference (RNAi) lines for the third ortholog. More than 50% of the RNAi plants showed fasciated inflorescence stems (**Fig. 5a–c**). RNAi specificity for *At3g25670* (hereafter called *AtFEA3*)

was confirmed by qRT–PCR (**Supplementary Fig. 15c**). As expected, the SAMs of these RNAi lines were enlarged (lines with strong knockdown, diameter of 294 ± 24 µm and lines with weak knockdown, 85 ± 12 µm, compared to 67 ± 7.6 µm for wild-type SAMs; *P* value < 0.001) (**Fig. 5d**,**e**). However, in contrast to known *clv* mutants[31–33] but similar to the maize *fea3* mutant, flower and silique development were normal (**Supplementary Fig. 15d–f**). This finding might explain why a mutant for this gene has not been characterized previously. We also asked whether *AtFEA3* RNAi plants showed altered sensitivity to CLE peptides[19]. Interestingly, as in maize *fea3* mutants, the *AtFEA3* RNAi lines did not show resistance to CLV3 but were resistant to a related CLE peptide, CLE27, in roots and in the SAM (**Fig. 5f**,**g**). *CLE27* is not the *ZmFCP1* ortholog (**Supplementary Fig. 5**). However, it is expressed similarly, at the SAM periphery and not in the central zone (**Supplementary Fig. 15g**). Our results indicate that FEA3 function is conserved in *Arabidopsis* and that FEA3 may perceive a CLE peptide that is produced in cells that are programmed for differentiation.

Weak *fea3* alleles enhance hybrid maize yield traits

We previously found that weak alleles of fasciated ear mutants could improve maize yield traits, such as kernel row number[34], by increasing the meristem size and number of primordia while maintaining the structural integrity of the meristem. To ask whether weak *fea3* alleles have similar effects, we backcrossed EMS alleles developed in our non-complementation screen to the W22 or B73 inbred line and generated F_1 hybrids. As expected, the B73 and W22 hybrids with the wild-type line had significantly enhanced yields when compared to the inbred lines, owing to heterosis ($P < 0.001$). We found that hybrids with the weak *fea3-2* and *fea3-3* alleles had further enhanced ear lengths, kernel row numbers, kernel numbers per ear, and ear weights (**Fig. 6**, **Supplementary Table 1** and **Supplementary Data 1**). The hybrids with these weak alleles were mildly fasciated but did not display the stunted ear growth that is normally associated with strongly fasciated mutants. These results are particularly exciting because, in our previous studies of weak *fea2* alleles, we found an increase in kernel row number but no overall increase in ear weight, owing to a compensatory reduction in kernel size[34]. Therefore, the newly identified *FEA3* signaling pathway could be used to develop new alleles for crop improvement.

DISCUSSION

Our results identify a conserved signaling system that has fundamentally different expression patterns and a distinct receptor–peptide combination as compared to the well-characterized *CLV–WUS* system. We hypothesize that this system allows feedback control of SAM size using a CLE signal expressed in differentiating primordia. Our model suggests that this new CLE signal moves from the organ primordia to the SAM, where it is perceived by FEA3; however, we cannot rule out the possibility of a secondary mobile signal, as the FEA3 receptor is also expressed in primordia. Indeed, such a caveat also applies to CLV3 because technical limitations have precluded the localization of CLV3 peptide *in vivo*. A feedback signaling system from primordia could provide control of stem cell proliferation and plant growth by integrating metabolic or other signals from the developing primordia. Weak alleles of *fea3* result in enhanced yield traits, as well as overall yield, in contrast to weak alleles of *fea2*, which increase kernel number without enhancing overall yield[34], suggesting that the weak alleles of *fea3* might also enhance sink strength in developing ears. A recent study also highlighted the importance of feedback signaling from progeny cells to the stem cell niche in mammalian hair follicles[35], suggesting that this may be a universal mechanism to control stem cell proliferation during development, with the potential to enhance crop yield traits.

URLs. Sequences and molecular markers are available from MaizeGDB at http://www.maizegdb.org/. Two-component driver system, http://maize.jcvi.org/cellgenomics/geneDB_list.php; FACS sorting data in the *Arabidopsis* eFP browser, http://bbc.botany.utoronto.ca/efp/cgi-bin/efpWeb.cgi; Python scientific package for modeling SciPy, http://www.scipy.org/.

METHODS

Methods and any associated references are available in the online version of the paper.

Accession codes. The *fea3-0* sequence is available from GenBank under accession KX009408.

Note: Any Supplementary Information and Source Data files are available in the online version of the paper.

ACKNOWLEDGMENTS

The *fea3-0* allele was kindly provided by V. Shcherbak (Krasnodar Research Institute of Agriculture). We also thank U. Hernandez for assistance with cloning, A. Masson for assistance with peptide assays, and members of the Jackson laboratory for comments on the manuscript. We acknowledge funding from a collaborative agreement with DuPont Pioneer and from NSF Plant Genome Research program grant IOS-1238202 and grant MCB-1027445 and from Agriculture and Food Research Initiative competitive grant 2016-67013-24572 of the USDA National Institute of Food and Agriculture. The study also received support from the Gatsby Charitable Foundation (GAT3395/PR4) and the Swedish Research Council (VR2013-4632) to H.J. and through the Next-Generation BioGreen 21 Program (SSAC; project PJ01184302) from the Rural Development Administration, Republic of Korea.

AUTHOR CONTRIBUTIONS

B.I.J. performed all experimental procedures except for those listed below, prepared figures, and wrote the draft of the manuscript. Y.K.L. and P.B. mapped and cloned *FEA3*. J.G. performed computational modeling, supervised by H.J. E.D.A. analyzed transactivation lines, using constructs generated by Q.W. A.L.E. performed expression analyses. A.G. performed *ZmWUS1* reporter line construction and characterization. R.M. provided the *ZmFCP1* mutants. M.B. performed phylogenetic analyses. M.K. and H.S. provided field genetics and mapping support and analysis. D.J. supervised the research and co-wrote the manuscript.

COMPETING FINANCIAL INTERESTS

The authors declare competing financial interests: details are available in the online version of the paper.

1. Morrison, S.J. & Spradling, A.C. Stem cells and niches: mechanisms that promote stem cell maintenance throughout life. *Cell* **132**, 598–611 (2008).
2. Heidstra, R. & Sabatini, S. Plant and animal stem cells: similar yet different. *Nat. Rev. Mol. Cell Biol.* **15**, 301–312 (2014).
3. Brand, U., Fletcher, J.C., Hobe, M., Meyerowitz, E.M. & Simon, R. Dependence of stem cell fate in *Arabidopsis* on a feedback loop regulated by CLV3 activity. *Science* **289**, 617–619 (2000).
4. Schoof, H. *et al.* The stem cell population of *Arabidopsis* shoot meristems in maintained by a regulatory loop between the *CLAVATA* and *WUSCHEL* genes. *Cell* **100**, 635–644 (2000).
5. Stahl, Y. & Simon, R. Plant primary meristems: shared functions and regulatory mechanisms. *Curr. Opin. Plant Biol.* **13**, 53–58 (2010).
6. Emery, J.F. *et al.* Radial patterning of *Arabidopsis* shoots by class III HD-ZIP and KANADI genes. *Curr. Biol.* **13**, 1768–1774 (2003).
7. Goldshmidt, A., Alvarez, J.P., Bowman, J.L. & Eshed, Y. Signals derived from *YABBY* gene activities in organ primordia regulate growth and partitioning of *Arabidopsis* shoot apical meristems. *Plant Cell* **20**, 1217–1230 (2008).
8. Tanaka, W. *et al.* The *YABBY* gene *TONGARI-BOUSHI1* is involved in lateral organ development and maintenance of meristem organization in the rice spikelet. *Plant Cell* **24**, 80–95 (2012).
9. Scanlon, M.J. The polar auxin transport inhibitor *N*-1-naphthylphthalamic acid disrupts leaf initiation, KNOX protein regulation, and formation of leaf margins in maize. *Plant Physiol.* **133**, 597–605 (2003).
10. Taguchi-Shiobara, F., Yuan, Z., Hake, S. & Jackson, D. The *fasciated ear2* gene encodes a leucine-rich repeat receptor-like protein that regulates shoot meristem proliferation in maize. *Genes Dev.* **15**, 2755–2766 (2001).

11. Jeong, S., Trotochaud, A.E. & Clark, S.E. The *Arabidopsis CLAVATA2* gene encodes a receptor-like protein required for the stability of the CLAVATA1 receptor-like kinase. *Plant Cell* **11**, 1925–1934 (1999).
12. Clark, S.E., Williams, R.W. & Meyerowitz, E.M. The *CLAVATA1* gene encodes a putative receptor kinase that controls shoot and floral meristem size in *Arabidopsis*. *Cell* **89**, 575–585 (1997).
13. Bommert, P. *et al. thick tassel dwarf1* encodes a putative maize ortholog of the *Arabidopsis CLAVATA1* leucine-rich repeat receptor-like kinase. *Development* **132**, 1235–1245 (2005).
14. Jackson, D., Veit, B. & Hake, S. Expression of maize KNOTTED1 related homeobox genes in the shoot apical meristem predicts patterns of morphogenesis in the vegetative shoot. *Development* **120**, 405–413 (1994).
15. Nimchuk, Z.L., Tarr, P.T., Ohno, C., Qu, X. & Meyerowitz, E.M. Plant stem cell signaling involves ligand-dependent trafficking of the CLAVATA1 receptor kinase. *Curr. Biol.* **21**, 345–352 (2011).
16. Lüscher, C. *et al.* Role of AMPA receptor cycling in synaptic transmission and plasticity. *Neuron* **24**, 649–658 (1999).
17. Fletcher, J.C., Brand, U., Running, M.P., Simon, R. & Meyerowitz, E.M. Signaling of cell fate decisions by CLAVATA3 in *Arabidopsis* shoot meristems. *Science* **283**, 1911–1914 (1999).
18. Nardmann, J. & Werr, W. The shoot stem cell niche in angiosperms: expression patterns of *WUS* orthologues in rice and maize imply major modifications in the course of mono- and dicot evolution. *Mol. Biol. Evol.* **23**, 2492–2504 (2006).
19. Kondo, T. *et al.* A plant peptide encoded by *CLV3* identified by *in situ* MALDI-TOF MS analysis. *Science* **313**, 845–848 (2006).
20. Ito, Y. *et al.* Dodeca-CLE peptides as suppressors of plant stem cell differentiation. *Science* **313**, 842–845 (2006).
21. Bommert, P., Je, B.I., Goldshmidt, A. & Jackson, D. The maize Gα gene *COMPACT PLANT2* functions in CLAVATA signalling to control shoot meristem size. *Nature* **502**, 555–558 (2013).
22. Opsahl-Ferstad, H.G., Le Deunff, E., Dumas, C. & Rogowsky, P.M. ZmEsr, a novel endosperm-specific gene expressed in a restricted region around the maize embryo. *Plant J.* **12**, 235–246 (1997).
23. Suzaki, T. *et al.* Conservation and diversification of meristem maintenance mechanism in *Oryza sativa*: function of the *FLORAL ORGAN NUMBER2* gene. *Plant Cell Physiol.* **47**, 1591–1602 (2006).
24. Suzaki, T., Yoshida, A. & Hirano, H.Y. Functional diversification of CLAVATA3-related CLE proteins in meristem maintenance in rice. *Plant Cell* **20**, 2049–2058 (2008).
25. McCarty, D.R. & Meeley, R.B. Transposon resources for forward and reverse genetics in maize. in *Handbook of Maize: Genetics and Genomics* (eds. Bennetzen, J.L. & Hake, S.C.) 561–584 (Springer Press, 2009).
26. Yadav, R.K. *et al.* Plant stem cell maintenance involves direct transcriptional repression of differentiation program. *Mol. Syst. Biol.* **9**, 654 (2013).
27. Chickarmane, V.S., Gordon, S.P., Tarr, P.T., Heisler, M.G. & Meyerowitz, E.M. Cytokinin signaling as a positional cue for patterning the apical–basal axis of the growing *Arabidopsis* shoot meristem. *Proc. Natl. Acad. Sci. USA* **109**, 4002–4007 (2012).
28. Gruel, J. *et al.* An epidermis-driven mechanism positions and scales stem cell niches in plants. *Sci. Adv.* **2**, e1500989 (2016).
29. Kinoshita, A. *et al.* RPK2 is an essential receptor-like kinase that transmits the CLV3 signal in *Arabidopsis*. *Development* **137**, 3911–3920 (2010).
30. Wu, Q., Luo, A., Zadrozny, T., Sylvester, A. & Jackson, D. Fluorescent protein marker lines in maize: generation and applications. *Int. J. Dev. Biol.* **57**, 535–543 (2013).
31. Clark, S.E., Running, M.P. & Meyerowitz, E.M. CLAVATA1, a regulator of meristem and flower development in *Arabidopsis*. *Development* **119**, 397–418 (1993).
32. Clark, S.E., Running, M.P. & Meyerowitz, E.M. CLAVATA3 is a specific regulator of shoot and floral meristem development affecting the same processes as CLAVATA1. *Development* **121**, 2057–2067 (1995).
33. Kayes, J.M. & Clark, S.E. CLAVATA2, a regulator of meristem and organ development in *Arabidopsis*. *Development* **125**, 3843–3851 (1998).
34. Bommert, P., Nagasawa, N.S. & Jackson, D. Quantitative variation in maize kernel row number is controlled by the *FASCIATED EAR2* locus. *Nat. Genet.* **45**, 334–337 (2013).
35. Hsu, Y.C., Li, L. & Fuchs, E. Transit-amplifying cells orchestrate stem cell activity and tissue regeneration. *Cell* **157**, 935–949 (2014).

ONLINE METHODS

Plant growth and map-based cloning. Maize plants were grown in the field or in the greenhouse. The original *fea3* allele, *fea3-0*, in an unknown genetic background, was crossed to the B73 inbred line and selfed to generate the F_2 population for bulked segregant mapping. One thousand mutants from the segregating F_2 population were used for map-based cloning with molecular markers available from MaizeGDB (*fea3-0* genotype data from the F_2 mapping population are provided in **Supplementary Data 2**). Phenotyping used the *fea3-0* allele, backcrossed seven times to the B73 inbred line. Additional alleles were identified using targeted EMS mutagenesis. To measure meristem size, segregating siblings were genotyped and the SAMs of 14-d-old plants (**Figs. 1a**,**b** and **4e**,**f**) or 28-d-old plants (**Fig. 3e**) were dissected, cleared, and measured as described previously[10]. All measurements for all experiments described in this manuscript included at least ten samples of each genotype with two or three independent biological replicates, and mean values ± s.d. are presented, with significance calculated using two-tailed, two-sample *t* tests; significant differences are reported as *P* values.

Meristem imaging and *in situ* hybridization. Scanning electron microscopy was performed on fresh tissues of maize and fixed tissues of *Arabidopsis* using a Hitachi S-3500N scanning electron microscope, as described[10]. *In situ* hybridization experiments were performed as described[14]. Antisense RNAs for *FEA3* and *ZmFCP1* were transcribed and used as probes. Primers are listed in **Supplementary Table 2**.

Transgene construction and imaging. The FEA3-RFP transgene was constructed by amplifying genomic fragments and fusing the RFP sequence in frame after the sequence for the signal peptide or the sequence encoding the C terminus, and the resulting constructs were transformed into maize. We used the MultiSite Gateway System (Invitrogen). All fragments were amplified using PhusionTaq polymerase (Finnzymes) and transferred to the pTF101 Gateway-compatible maize transformation vector by multisite LR recombination. Confirmed clones were transferred to *Agrobacterium* and transformed into maize, as described[36]. Primers are listed in **Supplementary Table 2**. To determine whether the FEA3-RFP construct could complement the *fea3-0* allele, primary FEA3-RFP transformants were crossed to homozygous *fea3-0* mutant plants, and F_1 plants that carried the FEA3-RFP transgene were backcrossed to homozygous *fea3-0* mutants. Sibling transgenic plants from these families were randomly crossed, and resulting families were subsequently analyzed for complementation. For genotyping, a 2.14-kb fragment from the *fea3-0* locus was amplified; the equivalent amplicon was a 1.96-kb fragment in wild type. The 1.96-kb PCR fragment also contained the site of RFP insertion, which allowed for simultaneous PCR detection of the transgene. The presence of the transgene locus was additionally monitored by Basta treatment of leaf tips. The *ZmWUS1* domain marker was developed by subcloning the sequences from 1,576 bp upstream of the GRMZM2G047448 gene ATG codon and 1,125 bp downstream of the stop codon into the MultiSite Gateway System. For a nucleus-localized fluorescent marker, four repeats of the Vir-E2 NLS sequence[37] were cloned in frame in front of the mRFP sequence[38], and the construct was subsequently subcloned into the MultiSite Gateway System. Primers are listed in **Supplementary Table 2**.

For confocal microscopy, tissues were dissected, counterstained with calcofluor white according to the manufacturer's instructions (Sigma-Aldrich, 18909) for 2 min, and imaged with a Zeiss LSM 710 microscope, using excitation at 561 nm and emission at 570–620 nm for RFP and excitation at 405 nm and emission at 450–500 nm for calcofluor white. Some tissues were treated with 2 μM D15 peptide[16] (the peptide sequence is listed in **Supplementary Table 3**) for 2 h before imaging.

Double-mutant analysis. Double mutants were constructed by crossing mutants introgressed into B73, followed by selfing or backcrossing to the F_1 progeny. All plants were subsequently genotyped (primers are listed in **Supplementary Table 2**). Plants were scored for spikelet density by counting the number of spikelets in a 2-cm region of the tassel central spike, after 2 cm had been removed from the tip. All genotype data for the double-mutant analysis are provided in **Supplementary Data 2**.

Protein extraction and detection. Aqueous two-phase partitioning was performed as described[21], using extracts from 1- to 2-cm maize ear primordia. To inhibit endocytosis, ear primordia were sliced into ~2-mm pieces and were treated with 1 mM D15 peptide for 2 h or underwent mock treatment with 1 mM randomized 15-mer peptide (the peptide sequence is listed in **Supplementary Table 3**) as a control. Samples from the upper and lower phases, enriched for plasma membrane and endoplasmic reticulum, respectively, were subjected to SDS–PAGE and immunoblotting. Blots were probed with antisera for RFP (Chromotek, 5F8), BiP lumenal binding protein (Agrisera, AS09-481), or plasma membrane H^+ ATPase (Agrisera, AS07-260), and signal was detected using a secondary horseradish peroxidase (HRP)-conjugated antibody (GE Healthcare), according to the manufacturer's instructions. This experiment was performed with two independent biological replicates.

Phylogenetic analysis. The amino acid sequences of the CLE proteins from *Arabidopsis*, maize, and rice were aligned using MUSCLE, and the resulting alignment was reverse-translated to DNA[39]. Only a very short region of the CLE proteins could be aligned with confidence; thus, the final alignment included only the functional ligand (**Supplementary Table 3**) plus two amino acids on either side. The DNA alignment (**Supplementary Data 3**) was partitioned into first, second, and third coding positions, and the best fitting model of sequence evolution and partitioning scheme was identified using PartitionFinder[40]. The alignment was analyzed both in its entirety and as two smaller alignments, corresponding to two frequently recovered clades. All alignments were analyzed using MrBayes v3.2.4, with model parameters allowed to vary between data partitions[41]. Two independent runs were initiated in each MrBayes analysis, and both were allowed to run for 10 million generations. The independent runs converged (s.d. of split frequencies <0.01) in all analyses.

Peptide assays. Maize embryos segregating for *fea3* and wild type were dissected at 10 d after pollination, when the SAM was exposed, and cultured on gel medium[21] containing scrambled peptide (30 μM; Genscript) or ZmFCP1, ESR2c, ZmCLE7, or ZmCLE14 peptide (peptide sequences are listed in **Supplementary Table 3**). After 10 d, embryos were collected for genotyping and fixed in FAA (10% formalin, 5% acetic acid, and 45% ethanol) and cleared in methyl salicylate. SAMs were measured by microscopy. Experiments used at least ten embryos per genotype and were replicated in triplicate. For measurement of root growth, mature seeds (**Supplementary Fig. 4**) or maize embryos dissected at 4 weeks after pollination segregating for wild type and the *fea3* mutant (**Supplementary Fig. 6a**) or segregating for the *fea3 fea2* double mutants (**Supplementary Fig. 6b**) were germinated on gel medium overnight. Synchronized germinating embryos were selected and transferred to gel medium in glass test tubes containing scrambled peptide (sCLV3; 5 or 10 μM; Genscript) or ESR2c, ZmFCP1, AtCLV3, ZmCLE7, CLE20, CLE40, ZmCLE21, or ZmCLE23 peptide (peptide sequences are listed in **Supplementary Table 3**). After 7 d, root length was measured; experiments were replicated in triplicate.

For measurement of *Arabidopsis* roots, sterilized seeds were cultured on half MS medium containing scrambled peptide (sCLV3; 1 μM) or AtCLV3, AtCLE25, AtCLE26, AtCLE27, or AtCLE45 peptide (peptide sequences are listed in **Supplementary Table 3**). After 10 d, root length was measured; the experiment was replicated in triplicate. For the measurement of *Arabidopsis* SAMs, sterilized seeds were cultured on half MS liquid medium containing CLV3 (1 μM), sCLV3 or CLE27, and the medium was renewed every third day. After 2 weeks, samples were collected, fixed and cleared, and SAMs were measured by microscopy. Peptide assays were completed with biological replicates performed by different investigators, and meristems were measured in a random order, before grouping based on genotype.

Two-components transactivation assays. The p*YABBY14*::*LhG4* driver line was constructed using the *ZmYABBY14* promoter (2,697 bp)[42] to drive LhG4 expression, and the p*Op*::*ZmFCP1* reporter line used the complete *ZmFCP1* coding region (925 bp). Fragments were cloned using the MultiSite Gateway System, as shown in **Supplementary Figure 8a** (ref. 43). Driver and reporter line heterozygotes were crossed to each other, and the families segregating the

doi:10.1038/ng.3567

two-component system were analyzed. Primers are listed in **Supplementary Table 2**. For real-time qPCR, dissected shoot apices (~2 × 2 × 3 mm) including SAM and young leaves were used.

Computational methods. The model includes the *CLV3–WUS* feedback loop and is a development from recent work for *Arabidopsis*[26,28,44]. It is fully described in the **Supplementary Note**.

In this system, *WUS* expression is activated by cytokinin, produced in the external cell layer[27], upon binding the AHK receptors[27,45]. The CLV3 peptide expressed in the stem cell niche represses *WUS* expression upon binding its receptor[46]; its own expression is activated by the diffusing transcription factor WUS[44].

The pattern of *ZmWUS1* expression in *fea3* (**Fig. 2d**) inside meristematic tissue and away from the epidermis offers insights into its regulation. Interestingly, this expression pattern mirrors the expression pattern of *AHK4* in *Arabidopsis*[27], suggesting that a similar cytokinin receptor could be present in maize, underlying *ZmWUS1* activation. In the following, we will consider the hypothetical expression pattern of *ZmAHK4* to be the inner tissue of the SAM. When activated by cytokinin, the receptor induces the expression of *ZmWUS1* in the model.

As previously shown, the positional information from the diffusion gradient of WUS alone is not sufficient to localize the *CLV3* expression domain at the tip of the shoot. In the present work, *CLV3* is co-activated by a signal originating from the epidermis, allowing the gene expression domains of WUS and CLV3 to mimic their wild-type expression patterns as well as those observed in a large set of mutants[26,44,47].

The model was imported to maize and adapted to include the experimental findings described in the main text. The model aims at understanding combined CLE signaling and the fasciation phenotype observed in the *fea3* mutant. The domain of activity of the wild-type *CLV3* promoter is used as a marker for the stem cell domain (central zone), and a large increase in its activity will be considered to lead to a fasciated phenotype[48].

The tissue template used for modeling is a three-dimensional representation of the maize SAM (**Supplementary Fig. 7**). The expression domains of genes of interest are defined from experimental data: *ZmWUS1* (**Fig. 2c** and ref. 18), *ZmCLE7* (hereafter referred to as *ZmCLV3*; phylogeny in **Supplementary Fig. 5**), *ZmAHK4* (ref. 49), *FEA3* (**Fig. 2b**), *ZmFCP1* (**Fig. 3c**), and also *ZmWUS1* expression in *fea3* (**Fig. 2d**).

A schematic of the model is shown in **Supplementary Figure 8**. *ZmWUS1* expression is driven by cytokinin binding the ZmAHK4 receptors. FEA3 receptors, upon binding ZmFCP1, and FEA2 receptors, upon binding either ZmCLV3 or ZmFCP1 (as supported by the peptide assays in **Fig. 3a** and **Supplementary Fig. 6b**), repress *ZmWUS1* expression. *FEA2* is constitutively expressed in the model[10]. ZmWUS1 and a hypothetical epidermis-originating signal activate *ZmCLV3* expression. Gene expression is modeled using Hill functions, and cell–cell transport of molecules is passive. The complete model is described by a set of seven differential equations for each cell of the tissue template (**Supplementary Note**).

The parameter values are inferred via an optimization strategy adapted from ref. 28 and making use of the CMA-ES algorithm[50]. Multiple optimizations resulted in 203 parameter sets successfully describing the wild-type expression of *ZmWUS1* and *ZmCLV3*. The model was further tested for loss of function of *ZmCLV3*, *FEA2*, *FEA3*, *FEA3 FEA2*, and *FCP1* and overexpression of *FCP1*. The variation in expression of both *ZmWUS1* and *ZmCLV3* under all conditions is presented in **Supplementary Figures 9** and **10**.

fea2, *fea3*, and *fea3 fea2* mutants all had a substantial increase in both *ZmWUS1* and *ZmCLV3* expression; the model thus predicts a fasciated phenotype for the three mutants, which proves to be consistent with the experimental data presented in **Figure 4**. Moreover, as shown, the severity of the phenotypes increases from *fea2* to *fea3* to *fea3 fea2*. Both the *fea3* and *fea3 fea2* mutants have a large downward expansion of the *ZmWUS1* domain, similar to the p*ZmWUS1*::*NLS.RFP* expression domain observed in *fea3* (**Fig. 2**).

The *fcp1* mutant has a large expansion in *ZmWUS1* and *ZmCLV3* expression and a predicted fasciated phenotype. The *ZmWUS1* domain exhibits a downward change in expansion typical of the *fea3* mutants.

Finally, overexpressing the *fcp1* peptide in its own expression domain (using a primordium-specific YABBY gene promoter) causes a decrease in *ZmWUS1* expression, leading to a reduction of *ZmCLV3* expression. The phenotype suggests a smaller stem cell pool and, thus, a reduction in the meristem size or meristem arrest.

The model described above is largely inspired by data obtained in *Arabidopsis*. In particular, the LOG genes, whose expression patterns are unknown in maize, are expressed in the epidermis; in rice, the expression resembles the stem cell domain[51]. To assess the importance of this choice, we modified the model such that the production of active cytokinin would not be limited to the epidermis but to the tip of the meristem, as suggested from the data obtained in rice.

This second 'rice-like' model was optimized in the same fashion as the previous model, resulting in 295 parameter sets. Strikingly, the model behaves extremely similarly to the '*Arabidopsis*-like' model (**Supplementary Figs. 11** and **12**), suggesting that the pattern of expression of the LOG genes in maize could be similar to that in either organism without affecting the conclusions of the present study.

***AtFEA3* RNAi and artificial microRNA construction.** For RNAi of *At3g25670*, the full-length cDNA or the 3′ UTR (289 bp) was cloned into the pHellsgate8 vector (SnapGene). The precursors for artificial miRNAs against *At3g25670* (**Supplementary Table 2**) were cloned into the miR-159a backbone following synthesis (Genscript) and were then mobilized into pDONR P4r-P3r using the Multisite Gateway System. Expression of the artificial miRNAs was driven by the *35S* promoter (p*35S*) or an *AGAMOUS* promoter (pAGm)[52]. All fragments were transferred to a modified pART27 Gateway-compatible *Arabidopsis* transformation vector by multisite LR recombination. Primers are listed in **Supplementary Table 2**. To measure meristem size, the SAMs of 14-d-old plants were dissected, cleared, and measured as described previously[10] (n = 16 (wild type and weak allele lines) and 8 (strong allele lines)).

Quantification of transcript abundance. qRT–PCR analysis was performed on a CFX96 Real-Time system (Bio-Rad), as described[53]. Total mRNA was extracted using an RNA extraction kit (Qiagen). Target cycle threshold values were normalized using *ZmUbiquitin* or *AtActin2*. Data are presented as the means of three biological replicates and three technical replicates. Primers are listed in **Supplementary Table 2**. RNA-seq reads from inflorescence meristem tips were obtained from wild-type and *fea3* mutant ear primordia as previously described[54]. Two biological replicates (pools of ~30 inflorescence meristem tips) were compared for wild type and *fea3* mutants. Reads were mapped to the maize reference genome (AGPv3) using TopHat 2 (ref. 55), and counts were normalized by the total number of reads mapped before plotting[56].

Yield trials. Lines carrying *fea3* EMS alleles developed in the non-complementation screen were backcrossed to W22 or B73 two to four times, and F_1 homozygous mutant hybrids were generated by crossing. Heterozygous *fea3-2* or *fea3-3* mutant hybrids were used as the control, 'normal' hybrids. Field tests were performed at Uplands Farm (Cold Spring Harbor, New York) in the summer of 2015. For analysis of yield parameters, 20–30 open-pollinated ears with a full seed set were analyzed.

36. Mohanty, A. *et al.* Advancing cell biology and functional genomics in maize using fluorescent protein–tagged lines. *Plant Physiol.* **149**, 601–605 (2009).
37. Crawford, K.M. & Zambryski, P.C. Subcellular localization determines the availability of non-targeted proteins to plasmodesmatal transport. *Curr. Biol.* **10**, 1032–1040 (2000).
38. Osterrieder, A. *et al.* Fluorescence lifetime imaging of interactions between Golgi tethering factors and small GTPases in plants. *Traffic* **10**, 1034–1046 (2009).
39. Edgar, R.C. MUSCLE: multiple sequence alignment with high accuracy and high throughput. *Nucleic Acids Res.* **32**, 1792–1797 (2004).
40. Lanfear, R., Calcott, B., Ho, S.Y. & Guindon, S. Partitionfinder: combined selection of partitioning schemes and substitution models for phylogenetic analyses. *Mol. Biol. Evol.* **29**, 1695–1701 (2012).
41. Ronquist, F. *et al.* MrBayes 3.2: efficient Bayesian phylogenetic inference and model choice across a large model space. *Syst. Biol.* **61**, 539–542 (2012).
42. Juarez, M.T., Twigg, R.W. & Timmermans, M.C. Specification of adaxial cell fate during maize leaf development. *Development* **131**, 4533–4544 (2004).
43. Krishnakumar, V. *et al.* A maize database resource that captures tissue-specific and subcellular-localized gene expression, via fluorescent tags and confocal imaging (Maize Cell Genomics Database). *Plant Cell Physiol.* **56**, e12(1–7) (2015).

44. Yadav, R.K. *et al.* WUSCHEL protein movement mediates stem cell homeostasis in the *Arabidopsis* shoot apex. *Genes Dev.* **25**, 2025–2030 (2011).
45. Gordon, S.P., Chickarmane, V.S., Ohno, C. & Meyerowitz, E.M. Multiple feedback loops through cytokinin signaling control stem cell number within the *Arabidopsis* shoot meristem. *Proc. Natl. Acad. Sci. USA* **106**, 16529–16534 (2009).
46. Ogawa, M., Shinohara, H., Sakagami, Y. & Matsubayashi, Y. *Arabidopsis* CLV3 peptide directly binds CLV1 ectodomain. *Science* **319**, 294 (2008).
47. Jönsson, H., Shapiro, B.E., Meyerowitz, E.M. & Mjolsness, E. Signalling in multicellular models of plant development. in *On Growth, Form and Computers* (eds. Kumar, S. & Bentley, P.J.) 156–161 (Elsevier Academic Press, 2003).
48. Iliev, I. & Kitin, P. Origin, morphology, and anatomy of fasciation in plants cultured *in vivo* and *in vitro*. *Plant Growth Regul.* **63**, 115–129 (2011).
49. Yonekura-Sakakibara, K., Kojima, M., Yamaya, T. & Sakakibara, H. Molecular characterization of cytokinin-responsive histidine kinases in maize. Differential ligand preferences and response to *cis*-zeatin. *Plant Physiol.* **134**, 1654–1661 (2004).
50. Hansen, N. The CMA evolution strategy: a comparing review. in *Towards a New Evolutionary Computation: Advances in Estimation of Distribution Algorithms* (eds. Lozano, J.A., Larrañga, P., Inza, I. & Bengoetxea, E.) 75–102 (Springer Press, 2006).
51. Kurakawa, T. *et al.* Direct control of shoot meristem activity by a cytokinin-activating enzyme. *Nature* **445**, 652–655 (2007).
52. Hong, R.L., Hamaguchi, L., Busch, M.A. & Weigel, D. Regulatory elements of the floral homeotic gene *AGAMOUS* identified by phylogenetic footprinting and shadowing. *Plant Cell* **15**, 1296–1309 (2003).
53. Whipple, C.J. *et al. grassy tillers1* promotes apical dominance in maize and responds to shade signals in the grasses. *Proc. Natl. Acad. Sci. USA* **108**, E506–E512 (2011).
54. Eveland, A.L. *et al.* Regulatory modules controlling maize inflorescence architecture. *Genome Res.* **24**, 431–443 (2014).
55. Kim, D. *et al.* TopHat2: accurate alignment of transcriptomes in the presence of insertions, deletions and gene fusions. *Genome Biol.* **14**, R36 (2013).
56. Trapnell, C. *et al.* Differential gene and transcript expression analysis of RNA-seq experiments with TopHat and Cufflinks. *Nat. Protoc.* **7**, 562–578 (2012).

doi:10.1038/ng.3567